# Bilirubin protects astrocytes from its own toxicity by inducing up-regulation and translocation of multidrug resistance-associated protein 1 (Mrp1)

Florinda Gennuso*†, Cristina Fernetti†‡, Cataldo Tirolo*, Nuccio Testa*, Francesca L'Episcopo*, Salvo Caniglia*, Maria Concetta Morale*, J. Donald Ostrow§, Lorella Pascolo‡, Claudio Tiribelli‡, and Bianca Marchetti*¶‖

*Neuropharmacology Section, OASI Institute for Research and Care on Mental Retardation and Brain Aging, 94018 Troina, Italy; ‡Liver Research Center, AREA Science Park and Department of Biochemistry, University of Trieste, 34127 Trieste, Italy; §Gastroenterology/Hepatology Division, Department of Medicine, University of Washington School of Medicine and Research Service (151L), Veterans Affairs Puget Sound Health Care System, Seattle, WA 98108-1597; and ¶Department of Pharmacology, Faculty of Medicine, University of Sassari, 07100 Sassari, Italy

Communicated by Rudi Schmid, University of California, San Francisco, CA, December 18, 2003 (received for review July 7, 2003)

**Unconjugated bilirubin (UCB) causes encephalopathy in severely jaundiced neonates by damaging astrocytes and neurons. Astrocytes, which help defend the brain against cytotoxic insults, express the ATP-dependent transporter, multidrug resistance-associated protein 1 (Mrp1), which mediates export of organic anions, probably including UCB. We therefore studied whether exposure to UCB affects the expression and intracellular localization of Mrp1 in cultured mouse astroglial cells (>95% astrocytes). Mrp1 was localized and quantitated by confocal laser scanning microscopy and double immunofluorescence labeling by using specific antibodies against Mrp1 and the astrocyte marker glial fibrillary acidic protein, plus the Golgi marker wheat germ agglutinin (WGA). In unexposed astrocytes, Mrp1 colocalized with WGA in the Golgi apparatus. Exposure to UCB at a low unbound concentration ($B_f$) of 40 nM caused rapid redistribution of Mrp1 from the Golgi throughout the cytoplasm to the plasma membrane, with a peak 5-fold increase in Mrp1 immunofluorescence intensity from 30 to 120 min. $B_f$ above aqueous saturation produced a similar but aborted response. Exposure to this higher $B_f$ for 16 h markedly decreased Trypan blue exclusion and methylthiazoletetrazoilum activity and increased apoptosis 5-fold by terminal deoxynucleotidyltransferase-mediated dUTP nick end labeling assay. These toxic effects were modestly increased by inhibition of Mrp1 activity with 3-([3-(2-[7-chloro-2-quinolinyl]ethenyl)phenyl-(3-dimethylamino-3-oxopropyl)-thio-methyl]thio)propanoic acid (MK571). By contrast, $B_f$ = 40 nM caused injury only if Mrp1 activity was inhibited by MK571, which also blocked translocation of Mrp1. Our conclusion is that in astrocytes, UCB up-regulates expression of Mrp1 and promotes its trafficking from the Golgi to the plasma membrane, thus moderating cytotoxicity from UCB, presumably by limiting its intracellular accumulation.**

Unconjugated bilirubin (UCB), the end product of heme catabolism in mammals, accumulates in the plasma of neonates, causing jaundice. Both *in vitro* and *in vivo*, UCB at low unbound concentrations ($B_f$) is a potent antioxidant that protects against damage from a wide range of oxidant agents (1–3). At $B_f$ modestly above its aqueous saturation (70 nM), however, *in vitro* exposure of astrocytes and neurons to UCB rapidly impairs a variety of cellular functions (4). In more severely jaundiced newborns, UCB accumulates in neurons and astroglial cells in selective brain regions, resulting in encephalopathy and kernicterus (5). The mechanism(s) by which severe hyperbilirubinemia engenders cytotoxic effects in selected brain regions is poorly understood but has been attributed previously to differences in permeability of the blood–brain barrier and the blood–cerebrospinal fluid barrier (6), regional blood flow (7), and rates of bilirubin oxidation (8).

Most cells are protected from accumulation of toxic compounds by active ATP-dependent export of the toxins, mediated by the ubiquitous multidrug resistance and multidrug resistance-associated protein (MRP) transporters, members of the superfamily of ATP-binding cassette (ABC) transporters (gene symbol *ABCC*) (9). Thus, rodent brain cell cultures, selectively enriched in astrocytes, microglia, oligodendrocytes, or neurones, have been shown to express various Mrp family members (10–12), and *MRP1* and *MRP5* mRNA have been detected in human brain endothelial cells (13). In rodents, Mrp1 is expressed in CNS barriers, the endothelial cells of brain microvessels (14), and the epithelial cells of the choroid plexus (15), and its importance in preventing CNS accumulation of various xenobiotics has been demonstrated in knockout mice (16, 17).

MRP1/Mrp1 is a major active transporter of glutathione, glucuronate, and sulfate conjugates (18) but can also transport unconjugated xenobiotics (19). UCB may be such an endogenous substrate, because ATP-dependent transport of UCB by vesicles of the yeast (*Saccharomyces cerevisiae*) is totally abolished in a double deletant strain lacking two homologues of MRP (20). Additionally, in a malignant choriocarcinoma (BeWo) cell line (21), ATP-dependent apical export of $^3$H-UCB has been correlated with apical expression of Mrp1 and is markedly decreased by the MRP-inhibitor, 3-([3-(2-[7-chloro-2-quinolinyl]ethenyl)-phenyl-(3-dimethylamino-3-oxopropyl)-thio-methyl]thio)propanoic acid (MK571).

Astrocytes defend neurons against oxidative insults (22, 23) by scavenging reactive oxygen species and producing factors that induce antioxidant enzymes (22–26). Astrocytes also regulate growth, differentiation, and survival of neurons as part of bidirectional neuronal–glial interactions (27–29). Efflux of glutathione from astroglial cells, mediated by Mrp1, is vital in the defense of CNS cells from antioxidants (30). Little is known, however, about the localization or functional modulation of MRP1/Mrp1 in astroglial cells, and the effects of UCB on this transporter have not been studied. We here report that, in cultured mouse astrocytes, Mrp1 is localized to the Golgi apparatus and that low concentrations of UCB rapidly up-regulate expression of Mrp1 and promote its translocation to the plasma membrane. We show also that this is associated with protection of astrocytes from cytotoxicity induced by UCB.

## Materials and Methods

**Bilirubin and Primary Antibodies.** UCB (Sigma) was purified as described by McDonagh and Assisi (31). Primary specific poly-

Abbreviations: UCB, unconjugated bilirubin; $B_f$, unbound UCB concentration; Mrp1, multidrug resistance-associated protein 1; GFAP, glial fibrillary acidic protein; GFAP-IR, GFAP immunoreactive; WGA-FITC, wheat-germ agglutinin labeled with FITC; TUNEL, terminal deoxynucleotidyltransferase-mediated dUTP nick end labeling; MK571, 3-([3-(2-[7-chloro-2-quinolinyl]ethenyl)phenyl-(3-dimethylamino-3-oxopropyl)-thio-methyl]thio)propanoic acid; DIV, days *in vitro*.

†F.G. and C.F. contributed equally to this work.

‖To whom correspondence should be addressed. E-mail: bianca.marchetti@oasi.en.it.





www.pnas.org/cgi/doi/10.1073/pnas.0308452100

clonal antibodies were: anti-Mrp1, prepared in our laboratory (32), and antiglial fibrillary acidic protein (GFAP) (goat antibodies against GFAP), from Santa Cruz Biotechnology. Wheat-germ agglutinin labeled with FITC (WGA-FITC) was obtained from Vector Laboratories.

**Astroglial Cell Cultures.** All experimental procedures were approved by the OASI Institution's review board. Primary astroglial cell cultures were obtained from mouse brains at postnatal days 1–2, according to Gallo *et al.* (27). Cells were seeded into 35-mm plastic Petri dishes or six-well plates (Costar) in nutrient medium [DMEM containing 10% heat-inactivated FCS, 2 mM glutamine, penicillin G (50 units/ml), and streptomycin (50 $\mu$g/ml)], at an initial density of 0.5–1 $\times$ $10^5$ cells/cm$^2$. The cultures were incubated in nutrient medium at 37°C under a humidified 5% $CO_2$/95% $O_2$ atmosphere. The medium was changed after 6 days and then twice per week. These glial cultures, characterized morphologically, biochemically, and immunocytochemically (27), were used at 14 days *in vitro* (DIV), when >95% of the cells were well differentiated and functional astrocytes, identified by their GFAP immunoreactivity (GFAP-IR) and survival and growth rates (see refs. 27 and 29 for overview).

**Astroglial Cell Treatments.** Under dim light, purified UCB was dissolved in DMSO and diluted with 100 volumes of culture medium containing 10% FCS. This solution was added to the cell cultures to yield final $B_f$ calculated to be 40 nM (low) and 145 nM (high).** A comparable volume of DMSO was added to the controls. After incubation for intervals from 5 min to 16 h, cells were fixed for immunofluorescent staining and coded samples analyzed blindly by confocal laser scanning microscopy.

**Immunocytochemistry.** For single and double immunofluorescence labeling, cells preincubated for 60 min in blocking buffer at 4°C (0.3–0.5% Triton X-100/5% BSA/5% normal serum in PBS) were then incubated overnight at 4°C with primary antibodies against Mrp1 (32) and GFAP, 1:100, as detailed elsewhere (27, 29). Golgi apparatus was stained with WGA-FITC (33). Specific FITC- and CY3-conjugated secondary antibodies were used at 1:100–1:200 dilution. Blanks were identically processed but with primary antibodies replaced by PBS.

**Confocal Laser Scanning Microscopy and Image Analysis.** Cells labeled by immunofluorescence were visualized and analyzed by using a Leica TCS NT (Ver. 1.0, Leica Lasertechnik, Heidelberg) inverted confocal laser scanning microscope equipped with an argon/krypton laser by using $\times$10, $\times$20, $\times$40, and $\times$100 oil-immersion objectives (27–29). The pinhole was set at 1.0–1.2 for optical sections of 0.5–0.6 $\mu$m. Single lower-power scans were followed by 16–22 serial optical sections of randomly chosen cells in four to five fields per coverslip by using the same settings. The average fluorescence (mean ± SD) intensity (pixel) in individual cell bodies or selected areas of each cell was measured throughout the stack (27).

To estimate Mrp1 fluorescence localized to the Golgi area, cells double-stained with anti-Mrp1 and WGA were acquired separately with the FITC and CY3 filters, and the intensity of Mrp1 fluorescence was determined in WGA-positive areas and corrected for background measured in areas devoid of cells. When added to wells both in the presence or absence of cells, UCB did not affect fluorescence intensity, either with or without MK571 present. Each condition was tested on a total of 60–80 cells, read from at least three cover slips obtained from at least two different cultures.

**Analysis of Cell Apoptosis.** Apoptotic DNA damage was identified in cells already immunostained with anti-GFAP by applying the terminal deoxynucleotidyltransferase-mediated dUTP nick end labeling (TUNEL) technique (*In Situ* Apoptosis Detection Kit, TACS TdT, R & D Systems). Confocal laser microscopy was applied on at least four randomly selected microscopic fields from a minimum of three different cover slips, examined at $\times$10, $\times$20, and $\times$40 objectives. Apoptotic cells (condensed chromatin, apoptotic bodies) were distinguished from necrotic cells (large nuclei, uncondensed chromatin) (27, 28). The numbers of apoptotic (TUNEL$^+$) GFAP-IR cells were expressed as a percentage of GFAP-IR cells (astrocytes) in the untreated control.

**Effects of Inhibition of Mrp1 Activity on UCB Cytotoxicity and Mrp1 Distribution in Astrocytes.** Cells cultured in 24-well plates for 14 DIV were exposed for 16 h to UCB at a calculated $B_f$ of 40 or 145 nM,** each in the absence or presence of 10 $\mu$M MK571, a specific inhibitor of MRP transporters (18). This nontoxic dose of MK571 was selected based on preliminary cytotoxicity studies at 1–50 $\mu$M (30). Cytotoxicity was assessed by four assays: (*i*) Cell viability by exclusion of Trypan blue (0.12% wt/vol) (27, 28); (*ii*) DNA labeling with fluorescent propidium iodide, 5 $\mu$g/ml (27–29) (the number of viable glial cells per unit area, expressed as a percentage of control cells treated with DMSO alone, was comparable by using both tests); (*iii*) mitochondrial integrity by the methylthiazoletetrazoilum test, according to the instructions of the manufacturer (Sigma–Aldrich); and (*iv*) apoptotic cells by TUNEL labeling (27, 28). Addition of UCB and/or MK571 to wells containing only cell-free medium indicated that neither compound interfered with these assays. For each experimental condition, at least three different cover slips were assessed on each of two cultures.

**Statistical Analyses.** Statistical significance between means ± SD was analyzed by two-way ANOVA. Experimental series performed on different days were compared by the Student–Newman–Keuls *t* test.

## Results

**Localization of Mrp1 to the Golgi Apparatus of Untreated Astrocytes (Fig. 1).** Mrp1 was detected in GFAP-positive astrocytes, localized asymmetrically in the perinuclear region of the cytoplasm, sparing the nucleus and the plasma membrane (Fig. 1*A*). Fusion of confocal images revealed minimal overlap between Mrp1 and the astrocyte cytoskeletal protein, GFAP, except in the perinuclear area (Fig. 1*B*). WGA-FITC revealed localization of the Golgi to the same perinuclear region (Fig. 1 *C* and *D*). The striking superimposition of the Mrp1 and Golgi markers in the perinuclear area (Fig. 1 *E* and *F*) confirmed the almost exclusive localization of the Mrp1 signal in the Golgi vesicles of astrocytes.

**Exposure of Astrocytes to UCB Induces Redistribution of Mrp1 from the Golgi Toward the Plasma Membrane (Figs. 2–4)** Exposure to UCB resulted in a time- and dose-dependent redistribution of the Mrp1 immunofluorescent signal (green) within GFAP-IR astrocytes (red). Between 5 and 10 min after addition of the low dose of UCB (Fig. 2 *A* and *D*), the Mrp1 signal had intensified but remained mainly in its asymmetric perinuclear location, characteristic of the Golgi. After 30 min of UCB

**$B_f$ was calculated by using equation 1 from Ostrow *et al.* (4), which used monomeric association constants derived from ultrafiltration studies (46) performed below the aqueous solubility limit for UCB. Above the solubility limit (70 nM) (34), self-aggregation of UCB causes this calculated $B_f$ to underestimate the total concentration of unbound UCB, which consists of monomers plus multimers of various sizes (47). Self-aggregation is likely to be limited at the calculated $B_f$ of 145 nM (47), which is approximately twice the solubility limit, so the error in the estimation of this $B_f$ is relatively small. The important concept is that this higher $B_f$ value is modestly above aqueous saturation of UCB, whereas the low $B_f$ value of 40 nM is below aqueous saturation.

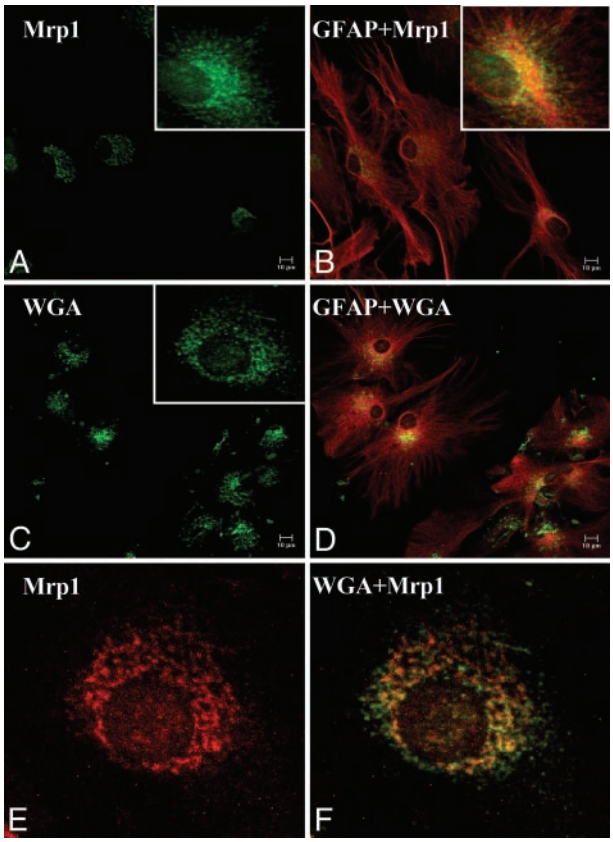


**Fig. 1.** Localization of Mrp1 in the Golgi apparatus of cultured mouse astrocytes. Immunofluorescence visualized in primary cultures of astroglial cells at 14 DIV by confocal laser scanning microscopy is shown. (Bars = 10 $\mu$m.) (*A* and *B*) Cells labeled with anti-Mrp1, revealed by FITC in green (*A*), with astrocyte architecture highlighted by anti-GFAP, revealed by CY3 in red (*B*). (*C* and *D*) Cells labeled with WGA-FITC (green) to highlight the Golgi apparatus (*C*) and with anti-GFAP (red) (*D*). (*E* and *F*) Cells labeled with anti-Mrp1 (red) (*E*) and WGA-FITC (green) (*F*). Fusion of confocal images between Mrp1 and WGA (orange and yellow dots, *F*) demonstrates the nearly complete overlap of the two labels in the perinuclear Golgi area.

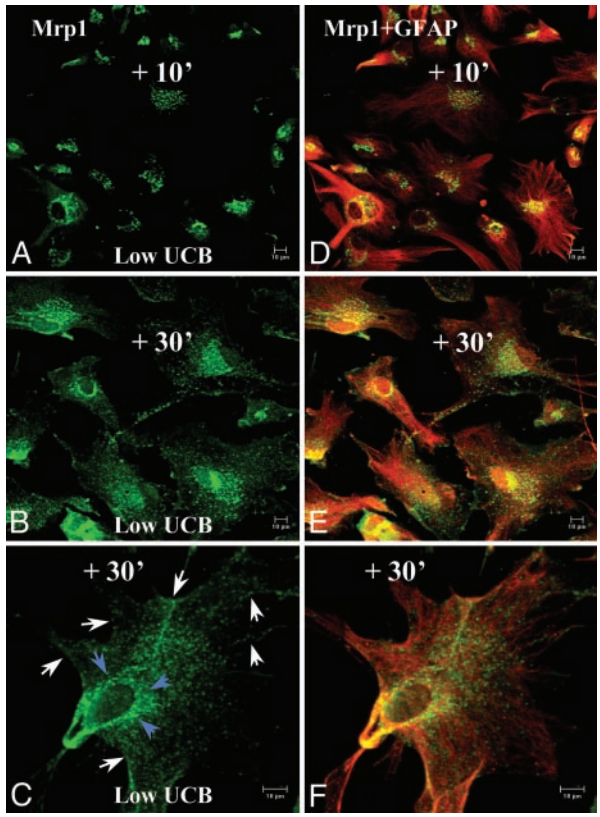


**Fig. 2.** A low concentration of UCB induces redistribution of Mrp1 in mouse astrocytes. Primary cultures of astroglial cells at 14 DIV were exposed to UCB at $B_f$ = 40 nM (low dose), and immunofluorescence was visualized by confocal laser microscopy. (Bars = 10 $\mu$m.) Cells were double-labeled with anti-Mrp1 (revealed by FITC in green) and anti-GFAP (revealed by CY3 in red). Ten-min (*A* and *D*) and 30-min (*B* and *E*) exposure to UCB, visualized at ×40 is shown. (*C* and *F*) Higher magnification (×100) at 30 min emphasizes a significant redistribution of Mrp1 from perinuclear Golgi regions (blue arrows) throughout the cell, including segments of the cell surface (white arrows). (*D–F*) Fusion images.

exposure (Fig. 2 *B*, *C*, *E*, and *F*), the Mrp1 signal had intensified markedly and spread throughout the cell cytoplasm, with some reaching the plasma membrane. Fusion images revealed extensive overlap between Mrp1 and GFAP, suggesting that migration of Mrp1 may have occurred along the astrocyte cytoskeleton. This major redistribution persisted for ≈90 min, whereas from 2 h on, the Mrp1 signal retreated progressively back to the asymmetrical perinuclear (Golgi) area, where it remained confined for the rest of the study (see supporting information, which is published on the PNAS web site). Double immunofluorescence labeling with WGA (green) and Mrp1 (red) indicated that, at 10 min (Fig. 3*A*), both markers had extended somewhat beyond the perinuclear area with partial overlap. At 30 min (Fig. 3*B*), there was nearly complete overlap between Mrp1 and WGA in the perinuclear area but also some overlap more peripherally, suggesting that some of the Mrp1 had migrated within translocated Golgi vesicles. From 4 h on, the almost complete overlap between the two markers persisted (see supporting information, which is published on the PNAS web site).

By contrast, application of the higher dose of UCB induced an aborted redistribution of Mrp1 immunofluorescence in astrocytes (Fig. 4). At 5 min, the Mrp1 signal intensified but remained localized in perinuclear Golgi-like regions (not shown). By 10 min (Fig. 4 *A* and *B*), Mrp1 immunofluorescence further intensified but now was spread throughout the cytoplasm and segments of the plasma membrane. By 30 min, however (Fig. 4 *C* and *D*), the Mrp1 signal was again almost exclusively localized in

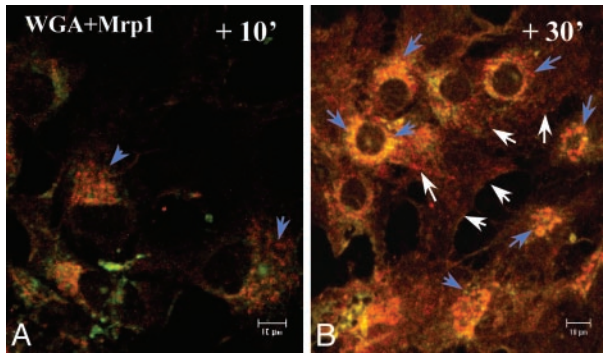


**Fig. 3.** Redistribution of Mrp1 and Golgi apparatus in astrocytes after exposure to a low concentration of UCB. Immunofluorescence was visualized by confocal laser scanning microscopy in primary cultures of astroglial cells exposed to low-dose UCB. (Bars = 10 $\mu$m.) Cells were double-labeled with anti-Mrp1 (revealed by CY3 in red) and with WGA (revealed by FITC in green) to highlight the Golgi apparatus. Fusion images at 10-min (*A*) and 30-min (*B*) exposure to UCB reveal considerable overlap between the two markers (yellow or orange) in the perinuclear area (blue arrows) and beyond (white arrows), with both entities more widespread throughout the cells at 30 min (*B*).

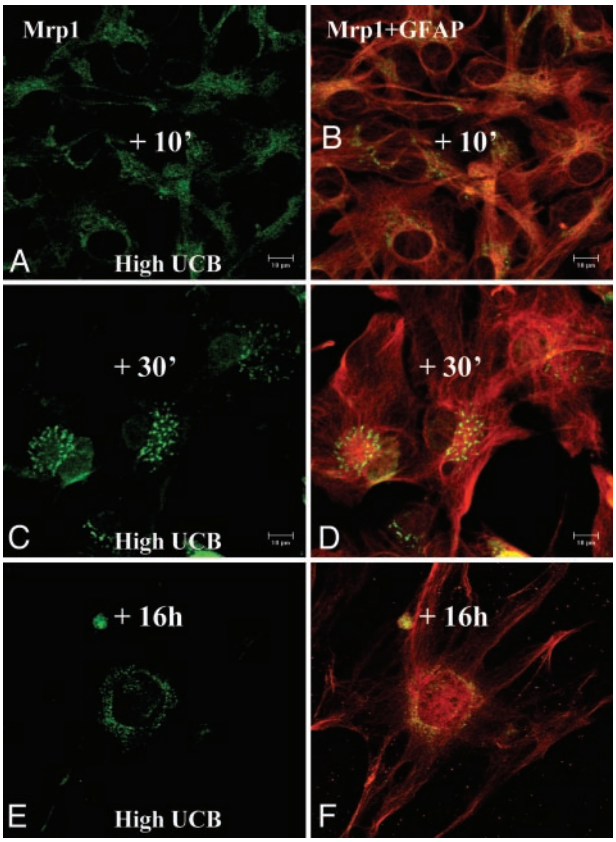


**Fig. 4.** Effect of exposure to the higher dose of UCB on the distribution of Mrp1 in mouse astrocytes. Primary cultures of astroglial cells at 14 DIV were exposed to the supersaturated higher dose of UCB (calculated $B_f$ = 145 nM), and immunofluorescence was visualized at 10 min, 30 min, and 16 h by confocal laser microscopy. (Bars = 10 $\mu$m.) Cells were double-labeled with anti-Mrp1 (revealed by FITC in green) plus GFAP (revealed by CY3 in red) to highlight astrocyte architecture, with fusion images (yellow) at right in *B*, *D*, and *F*. (*A* and *B*) At 10 min, Mrp1 immunofluorescent signal intensity is increased and has migrated throughout the cell. By 30 min (*C* and *D*) and for the entire experimental period (*E* and *F*), however, the Mrp1 signal has retreated and once again localizes only in the Golgi area.

the Golgi in a coarsely granular pattern, where it remained for the 16-h duration of the study, albeit with a lower fluorescence intensity (Fig. 4 *E* and *F*).

**UCB Increases the Mrp1 Immunofluorescent Signal in Astrocytes (Fig. 5).** Application of either the low or higher dose of UCB induced a steep increase in Mrp1 fluorescence intensity by 30 min, both in WGA-positive Golgi areas and throughout the cell cytoplasm (not shown), although the timing differed between the two doses. With the low dose of UCB, an almost 5-fold increase of Mrp1 immunofluorescence within the Golgi at 30 min accompanied the Mrp1 redistribution throughout the cell cytoplasm. A plateau was then maintained until 2 h, after which the Mrp1 fluorescence intensity decreased by almost 50% to reach a new plateau from 4 to 8 h; it then returned to control values by 16 h. By contrast, after application of the higher dose of UCB, the comparable 5-fold increase of fluorescence intensity declined rapidly after the sharp peak at 30 min, returned to control levels after 4–8 h, and fell below those levels by 16 h. Comparable time- and dose-dependent changes were observed when Mrp1 expression was analyzed at a single-cell level, in the $GFAP^+$ cell subset, by using flow cytometric analysis (see supporting information).

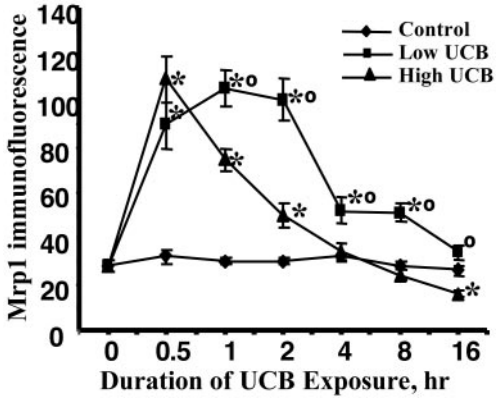


**Fig. 5.** UCB induces up-regulation of the Mrp1 immunofluorescent signal in cultured mouse astrocytes. Astroglial cells incubated with UCB at several $B_f$ values were serially processed for double-immunofluorescent staining with anti-Mrp1 plus WGA to highlight the Golgi apparatus and analyzed by confocal laser scanning microscopy. Mrp1 fluorescence (mean ± SD) intensity (pixel) localizing to the Golgi area is plotted on the *y* axis against a nonlinear time scale on the *x* axis. Cells incubated without UCB (control) showed no changes in Mrp1-immunofluorescence over 16 h, whereas a 4-fold increase occurred by 30 min in cells treated with low- or higher-dose UCB. After 30 min, the up-regulation declined much more rapidly in cells exposed to the higher dose of UCB. *, $P < 0.01$ vs. untreated controls at each respective time; ○, $P < 0.01$ vs. higher dose of UCB.

**Inhibition of Mrp1 with MK571 Prevents Mrp1 Translocation and Increases the Vulnerability of Astrocytes to UCB-Induced Cytotoxicity (Fig. 6).** In the absence of MK571, a specific inhibitor of Mrp transporters (18), exposure to the low dose of UCB did not significantly modify: cell survival, measured by trypan blue exclusion (Fig. 6*A*), or nuclear staining with the dye propidium iodide (PI) (not shown); mitochondrial activity, assessed by the methylthiazoletetrazoilum reduction assay (Fig. 6*B*); or apoptosis, measured by TUNEL assay (Fig. 6*C*). On the other hand, the higher dose of UCB significantly impaired all these astroglial functions and cell survival: astrocytes appeared shriveled and clumped together; Trypan blue exclusion, PI staining of nuclei, and mitochondrial activity all decreased by 55–64%; and the proportion of apoptotic cells increased to about five times control levels (all $P < 0.01$). Addition of MK571 (10 $\mu$M) alone did not affect cell viability but significantly accentuated the impairment of cell function and viability induced by the higher concentration of UCB (Fig. 6 *A–C*). At the low dose of UCB, which produced no toxicity by itself, addition of MK571 engendered impairment of cell function and viability comparable to those observed with the higher dose of UCB alone (Fig. 6 *A–C*).

Although MK571 alone did not affect the distribution of the Mrp1, WGA-FITC or GFAP immunofluorescent signals, it blocked the early redistribution of the Mrp1 immunofluorescent signal induced by the low dose of UCB (compare Fig. 6*D* with Fig. 2 *E* and *F*). Indeed, in the presence of MK571, Mrp1 remained confined to its Golgi-perinuclear location throughout the 16 h of the study (Fig. 6*F*), similar to what was observed after 30 min of exposure to higher dose UCB without MK571 (compare Fig. 6 *D* and *F* with Fig. 4 *C–F*). With the higher dose of UCB + MK571, the Mrp1 never left the Golgi from 5 min through 16 h (Fig. 6*E* shows the situation at 30 min). Thus, inhibition by MK571, of the function and intracellular redistribution of Mrp1, increased the vulnerability of astroglia to the cytotoxic effects of a supersaturating concentration of unbound UCB, prevented the migration of Mrp1 toward the plasma membrane, and rendered these cells susceptible to toxic effects of UCB at a concentration below saturation.

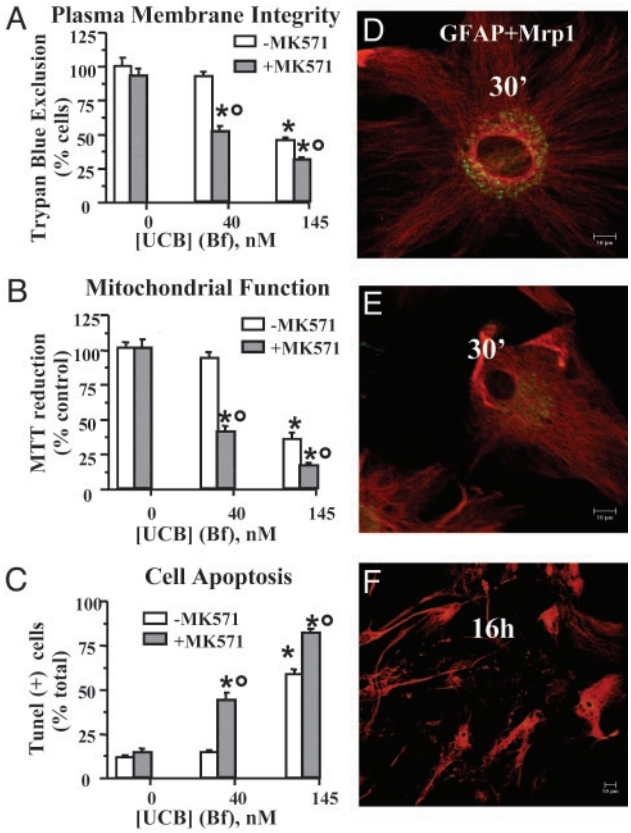


**Fig. 6.** Inhibition of Mrp1 activity by MK571 prevents Mrp1 redistribution and increases vulnerability of astroglia to bilirubin cytotoxicity. Astroglial cells maintained in culture for 14 DIV were exposed for 16 h to either low- or higher-dose UCB, in the absence (white bars) or the presence (black bars) of the Mrp inhibitor, MK571. Control incubations contained no UCB. (*A*) Trypan blue exclusion to assess plasma membrane integrity. (*B*) Methylthiazoletetrazoilum reduction to monitor mitochondrial function. (*C*) TUNEL test to identify DNA damage in apoptotic cells. In *A* and *B*, the results are expressed as percent of control incubations in the absence of UCB and MK571. *, $P < 0.01$ vs. MK571 control; ○, $P < 0.01$ vs. higher-dose UCB. (*D–F*) Confocal laser scanning microscopy of cell cultures after treatment with UCB + MK571, processed for double-immunofluorescent staining with anti-GFAP (red) and anti-Mrp1 (green). The migration of Mrp1 outward from Golgi in response to low dose UCB (see Fig. 2 *B*, *C*, *E*, and *F*) was inhibited by added MK571 at 30 min (*D*) and 16 h (*F*), and cells at 16 h appeared severely shriveled. With higher-dose UCB + MK571, the Mrp1 remained confined to the Golgi (*E* shows the situation at 30 min).

## Discussion

By using a specific antibody against Mrp1 (32) and by combining immunocytochemistry with confocal laser scanning microscopy to investigate the intracellular fate of Mrp1 in primary cultures of mouse astroglial cells, we demonstrated that, in GFAP-IR astrocytes: (*i*) Mrp1 is asymmetrically localized to the perinuclear region within the Golgi apparatus; (*ii*) exposure to UCB at low concentrations (calculated $B_f = 40$ or 145 nM) dramatically and rapidly up-regulates the Mrp1 immunofluorescent signal and promotes extensive trafficking of this ATP-dependent transporter to the plasma membrane in a dose- and time-dependent fashion; (*iii*) blocking Mrp efflux pumps with MK571: (*a*) inhibits the trafficking of Mrp1, (*b*) increases the susceptibility of these cells to the toxic effects of unbound UCB at a concentration (higher dose) modestly above aqueous saturation, and (*c*) even renders astrocytes vulnerable to membrane, mitochondrial, and nuclear damage at a normally nontoxic $B_f$ of 40 nM (low dose), that is below aqueous saturation (34).

In contrast with the rapid and persistent up-regulation and translocation of Mrp1 at the lower concentration of UCB was the transience of these phenomena at the higher supersaturating concentration of UCB, with a steep decline in Mrp1 expression after the 30-min peak and limited and aborted migration of Mrp1 to the plasma membrane. This impaired response of Mrp1 probably contributes to the inability of astrocytes to protect themselves against the cytotoxicity of concentrations of unbound UCB above aqueous saturation (4). Consistent with this suggestion, blocking the up-regulation, migration, and function of Mrp1 with MK571 dramatically increased vulnerability of astrocytes even to the lower $B_f$ of 40 nM, which is only twice the physiological $B_f$ level in plasma.

UCB-induced up-regulation and redistribution of Mrp1 from the Golgi to the plasma and nuclear membrane, where it could pump neurotoxins out of the cytoplasm and nucleus respectively, are reminiscent of findings in cells rendered multidrug-resistant by repeated exposure to chemotherapeutic agents. In such cells, expression of P-glycoprotein (PgP) (MDR1/Mdr1) has been reported in the nucleus (35), in the Golgi apparatus and plasma membrane (33), whereas untreated human melanoma cells express both , PgP and Mrp1 drug transporters mainly in the Golgi (36). The comparable response of Mrp1 to UCB presumably limits intracellular accumulation of this pigment. This is in line with previous evidence in yeast (20) and placental trophoblasts (21, 37) suggesting that Mrp1 may be involved in the ATP-dependent transport of UCB. It is supported further by our recent demonstration that rats rendered hyperbilirubinemic by hemolysis induced with phenylhydrazine exhibit up-regulation of Mrp1 mRNA and protein in the liver and spleen, and that this response is blunted by decreasing UCB formation with the heme oxygenase inhibitor, tin mesoporphyrin (38).

We propose that Mrp1 is an important protector against UCB toxicity in the many cells in which it is expressed, most importantly in the CNS (9). In the blood–brain barrier (brain capillary endothelial cells) and blood–cerebrospinal fluid barrier (choroid plexus epithelial cells), together with other ATP-binding cassette transporters such as MDR1 (39), MRP1/Mrp1 plays a major role in extruding drugs and other xenobiotics from the CNS (16, 17, 40). It is logical that a similar mechanism(s) regulates the intracellular concentrations of UCB, which is neuroprotective against antioxidant stress at $B_f$ below the aqueous phase solubility limit of 70 nM (1) but impairs multiple functions of neurons and astrocytes at $B_f$ only modestly above aqueous saturation (4).

Astrocytes are of prime importance in maintaining the integrity of the blood–brain barrier (41). Of special interest, astrocytes play crucial roles in the brain response to neuronal injury and plasticity (23, 24, 26). In particular, functional astrocytes are required to defend neurons against reactive oxygen and nitrogen species, whereas loss of astrocyte function increases neuronal vulnerability to cell death (24, 26). The modulation by UCB of the expression and localization of the Mrp1 efflux pump in astrocytes, herein reported, may thus be pivotal for protecting neurons against toxic insults, such as oxidant stress (26) and UCB itself.

## Conclusion

In conclusion, our results add Mrp1 to the list of enzymes and transporters whose expression is regulated by UCB (42). Although the mechanism(s) of this up-regulation remains to be clarified, this study clearly shows that UCB, at even slightly elevated $B_f$ levels, promotes a marked up-regulation and membrane targeting of the multidrug resistance-associated protein transporter, Mrp1, in mouse astrocytes, and that blocking Mrp1 function dramatically prevents this adaptive response and increases the vulnerability of astroglial cells to

UCB-induced damage. Thus, UCB, by modifying its own export, appears to provide astroglial and possibly other CNS cells with a measure of resistance against its own cytotoxicity. Preservation or stimulation of this export function of Mrp1 offers a potential approach to prevention and treatment of bilirubin encephalopathy in newborn infants, in whom the "physiological jaundice of the newborn" is believed to be neuroprotective (2) but in whom more severe/prolonged hyperbilirubinemia may damage selected focal areas of the CNS (43–45).

This work was supported by grants from the Italian Ministry of Health (Strategic Research Project RF-2002, contract no. 189), Italian Ministry of Research, OASI Institute for Research and Care on Mental Retardation and Brain Aging Troina (Enna) Italy to B.M., by grants from Fondo Studio Fegato Trieste, Italy (C. Tiribelli), and by career development awards from Bracco Italy (C.F. and L.P.).

1. Dore, S. & Snyder, S. H. (1999) *Ann. N.Y. Acad. Sci.* **890,** 167–172.
2. Dore, S., Takahashi, M., Ferris, C. D., Zakhary, R., Hester, L. D., Guastella, D. & Snyder, S. H. (1999) *Proc. Natl. Acad. Sci. USA* **96,** 2445–2450.
3. Tomaro, M. L. & Batlle, A. M. D. (2002) *Int. J. Biochem. Cell Biol.* **34,** 216–220.
4. Ostrow, J. D., Pascolo, L. & Tiribelli, C. (2003) *Pediatr. Res.* **54,** 98–104.
5. Gourley, G. R. (1997) *Adv. Pediatr.* **44,** 173–229.
6. Wennberg, R. P. (2000) *Cell Mol. Neurobiol.* **20,** 97–109.
7. Burgess, G. H., Oh, W., Bratlid, D., Brubakk, A. M., Cashore, W. J. & Stonestreet, B. S. (1985) *Pediatr. Res.* **19,** 691–696.
8. Hansen, T. W. R. (2000) *Mol. Genet. Metab.* **71,** 411–417.
9. Borst, P., Evers, R., Kool, M. & Wijnholds, J. (1999) *Biochim. Biophys. Acta* **1461,** 347–357.
10. Rao, V. V., Dahlheimer, J. L., Bardgett, M. E., Snyder, A. Z., Finch, R. A., Sartorelli, A. C. & Piwnica-Worms, D. (1999) *Proc. Natl. Acad. Sci. USA* **96,** 3900–3905.
11. Hirrlinger, J., König, J. & Dringen, R. (2002) *J. Neurochem.* **82,** 716–719.
12. Decleves, X., Regina, A., Laplanche, J. L., Roux, F., Boval, B., Launay, J. M. & Scherrmann, J. M. (2000) *J. Neurosci. Res.* **60,** 594–601.
13. Kool, M., de Haas, M., Scheffer, G. L., Scheper, R. J., van Eijk, M. J., Juijn, J. A., Baas, F. & Borst, P. (1997) *Cancer Res.* **57,** 3537–3547.
14. Seetharaman, S., Barrand, M. A., Maskell, L. & Scheper, R. J. (1998) *J. Neurochem.* **70,** 1151–1159.
15. Regina, A., Koman, A., Piciotti, M., El Hafny, B., Center, M. S., Bergmann, R., Couraud, P. O. & Roux, F. (1998) *J. Neurochem.* **71,** 705–715.
16. Wijnholds, J., de Lange, E. C., Scheffer, G. L., van Den Berg, D. J., Mol, C. A. A. M., van der Valk, M. A., Schinkel, A. H., Scheper, R. J., Breimer, D. D. & Borst, P. (2000) *J. Clin. Invest.* **105,** 279–285.
17. Ghersi-Egea, J. F. & Strazielle, N. (2001) *Microsc. Res. Technol.* **52,** 83–88.
18. Leier, I., Jedlitschky, G., Buchholz, U., Center, M. S., Cole, S. P., Deeley, R. G. & Keppler, D. (1996) *Biochem. J.* **314,** 433–437.
19. Zaman, G. J. R., Lankelma, J., Vantellingen, O., Beijnen, J. H., Dekker, H., Paulusma, C. C., Oude Elferink, R. P. J., Baas, F. & Borst, P. (1995) *Proc. Natl. Acad. Sci. USA* **92,** 7690–7694.
20. Petrovic, S., Pascolo, L., Gallo, R., Cupelli, F., Ostrow, J. D., Goffeau, A., Tiribelli, C. & Bruschi, C. V. (2000) *Yeast* **16,** 561–571.
21. Pascolo, L., Fernetti, C., Crivellato, E., Garcia-Mediavilla, M. V., Ostrow, J. D. & Tiribelli, C. (2001) *FEBS Lett.* **495,** 94–99.
22. Dringen, R. (2000) *Prog. Neurobiol.* **62,** 649–671.
23. Marchetti, B., Morale, M. C., Testa, N., Tirolo, C., Caniglia, S., Amor, S., Dijkstra, C. D. & Barden, N. (2001) *Brain Res. Rev.* **37,** 259–272.
24. McNaught, K. S. P. & Jenner, P. (1999) *J. Neurochem.* **73,** 2469–2476.
25. Kussmaul, L., Hamprecht, B. & Dringen, R. (1999) *J. Neurochem.* **73,** 1246–1253.
26. Morale, M. C., Serra, P. A., Delogu, M. R., Migheli, R., Rocchitta, G., Tirolo, C., Caniglia, S., Testa, N., L'Episcopo, F., Gennuso, F., *et al.* (2004) *FASEB J.* **18,** 164–166.
27. Gallo, F., Morale, M. C., Spina-Purrello, V., Tirolo, C., Testa, N., Farinella, Z., Avola, R., Beaudet, A. & Marchetti, B. (2000) *Synapse* **36,** 233–253.
28. Gallo, F., Morale, M. C., Tirolo, C., Testa, N., Farinella, Z., Avola, R., Beaudet, A. & Marchetti, B. (2000) *J. Neuroendocrinol.* **12,** 941–959.
29. Avola, R., Spina-Purrello, V., Gallo, F., Morale, M. C., Marletta, N., Costa, A., Tirolo, C., Testa, N., Reale, S. & Marchetti, B. (2000) *Int. J. Dev. Neurosci.* **18,** 743–763.
30. Hirrlinger, J., Resch, A., Gutterer, J. M. & Dringen, R. (2002) *J. Neurochem.* **82,** 635–644.
31. McDonagh, A. F. & Assisi, F. (1972) *Biochem. J.* **129,** 797–800.
32. Fernetti, C., Pascolo, L., Podda, E., Gennaro, R., Stebel, M. & Tiribelli, C. (2001) *Biochem. Biophys. Res. Commun.* **288,** 1064–1068.
33. Molinari, A., Cianfriglia, M., Meschini, S., Calcabrini, A. & Arancia, G. (1994) *Int. J. Cancer* **59,** 789–795.
34. Hahm, J. S., Ostrow, J. D., Mukerjee, P. & Celic, L. (1993) *J. Lipid Res.* **33,** 1123–1137.
35. Baldini, N., Scotlandi, K., Serra, M., Shikita, T., Zini, N., Ognibene, A., Santi, S., Ferracini, R. & Maraldi, N. M. (1995) *Eur. J. Cell Biol.* **68,** 226–239.
36. Molinari, A., Calcabrini, A., Meschini, S., Stringaro, A., Del Bufalo, D., Cianfriglia, M. & Arancia, G. (1998) *Int. J. Cancer* **75,** 885–893.
37. Serrano, M. A., Bayón, J. E., Pascolo, L., Tiribelli, C., Ostrow, J. D., Gonzalez-Gallego, J. & Marin, J. J. G. (2002) *Placenta* **23,** 527–535.
38. Cekic, D., Bellarosa, S., Garcia-Mediavilla, M. V., Rigato, I., Pascolo, L., Ostrow, J. D. & Tiribelli, C. (2003) *Biochem. Biophys. Res. Commun.* **311,** 891–896.
39. Cordon-Cardo, C., O'Brien, J. P., Casals, D., Rittman-Grauer, L., Biedler, J. L., Melamed, M. R. & Bertino, J. R. (1989) *Proc. Natl. Acad. Sci. USA* **86,** 695–698.
40. Ostrow, J. D., Pascolo, L., Shapiro, S. M. & Tiribelli, C. (2003) *Eur. J. Clin. Invest.* **33,** 988–997.
41. Descamps, L., Coisne, C., Dehouck, B., Cecchelli, R. & Torpier, G. (2003) *Glia* **42,** 46–58.
42. Huang, W., Zhang, J., Chua, S. S., Qatanani, M., Han, Y., Granata, R. & Moore, D. D. (2003) *Proc. Natl. Acad. Sci. USA* **100,** 4156–4161.
43. Schutta, H. S. & Johnson, L. H. (1967) *J. Neuropathol. Exp. Neurol.* **26,** 377–396.
44. Sawasaki, Y., Yamada, N. & Nakajima, H. (1976) *J. Neurochem.* **27,** 577–583.
45. Jew, J. Y. & Sandquist, D. (1979) *Arch. Neurol.* **36,** 149–154.
46. Weisiger, R. A., Ostrow, J. D., Koehler, R. K., Webster, C. C., Mukerjee, P., Pascolo, L. & Tiribelli, C. (2001) *J. Biol. Chem.* **276,** 29953–29960.
47. Mukerjee, P., Ostrow, J. D. & Tiribelli, C. (2002) *BMC Biochem.* **3,** 17.